Dalton Transactions

PAPER

View Article Online
View Journal | View Issue

Check for updates

Cite this: *Dalton Trans.*, 2018, **47**, 5771

Phosphate glasses *via* coacervation route containing $CdFe_2O_4$ nanoparticles: structural, optical and magnetic characterization†

Juliane R. Orives, *[a] Wesley R. Viali, [a] Silvia H. Santagneli, [a] Conrado R. M. Afonso, [b] Maria H. Carvalho, [c] Adilson J. A. de Oliveira [c] and Marcelo Nalin [a]

Received 9th February 2018,
Accepted 25th March 2018

DOI: 10.1039/c8dt00560e

rsc.li/dalton

$CdFe_2O_4$ nanoparticles of around 3.9 nm were synthesized using the coprecipitation method and protected by a silica layer. The nanoparticles were mixed with a coacervate and transformed into phosphate glasses with 1, 4 and 8% in mass of nanoparticles by the melt-quenching method. TEM images confirm that the nanoparticles were successfully incorporated into the matrix without inducing crystallization. ^{31}P NMR and Raman spectral analyses show that new P–O–Si bonds are formed in the glasses containing nanoparticles. The glass transition increases as a function of the nanoparticle content due to an increase in the connectivity of the phosphate glass chains. The UV-Vis spectra show bands at 415 and 520 nm assigned to Fe^{3+} ions and at 1025 nm, characteristic of Fe^{2+} ions, indicating that some of the nanoparticles dissolve during the melting process. The sample with 8% $CdFe_2O_4$ presents a paramagnetic behavior. The glasses obtained are transparent, non-hygroscopic and possess enormous thermal stability which is important for the production of optical devices.

1 Introduction

Phosphate glasses present important characteristics for optics such as high transparency in UV-Vis, low glass transition temperature (T_g) and low melting point (T_m) compared to silicate glasses.[1,2]

These glasses can be successfully obtained *via* coacervation process, which involves the interaction of a solution of sodium polyphosphate, $Na(PO_3)_n$, with divalent ions, such as Ca^{2+} and Zn^{2+}.[3,4] This interaction results in a phase separation process where the colloidal richest phase is called the coacervate, while the less viscous phase is the supernatant.[5–7] The coacervation method has shown great results in producing phosphate glasses for optical applications.[8]

From the coacervation process, it is possible to incorporate ions or nanoparticles into the phosphate structure at room temperature and, because it is a compound that before drying has a gel appearance, homogenization occurs efficiently. After incorporation of the nanoparticles of interest (such as nanoparticles with plasmonic or magnetic properties, for example) it is possible to transform this material into glass using a melting process followed by rapid cooling.[4,9]

The main methods to obtain nanoparticles in glasses are the growth of the nanoparticles by laser irradiation or growth by thermal treatment, where the matrices which contain the necessary precursors for the formation of nanoparticles are obtained first by the melt-quenching method.[10–15] Some disadvantages of these methods are the lack of control of nanoparticle size and homogeneity throughout the matrix, since growth may be favored on the surface or at certain points of the samples.

Recently, the method for incorporation of nanoparticles *via* the melt-quenching process has been used, in which the nanoparticles are mixed with the precursors of the glass and then the material is melted. The further steps of growth *via* laser or thermal treatment are not necessary.[16–20]

Glasses containing iron oxide nanoparticles obtained from natural sand with an average size of 70 nm have been reported in the literature; after glass synthesis, the nanoparticles presented an average size of 26 nm, as observed by transmission electron microscopy (TEM).[16–18]

Farag and Marzouk[19] incorporated NiO nanoparticles of 70 nm synthesized by the sonochemical method in sodium zinc borate glasses, while Chen *et al.*[20] synthesized iron oxide

[a]*Institute of Chemistry – São Paulo State University – UNESP, P. O. Box 355, Araraquara, SP, 14800-060, Brazil. E-mail: juliane_resges@hotmail.com*
[b]*Department of Materials Engineering (DEMa), Federal University of São Carlos (UFSCar), São Carlos, SP, 13565-905, Brazil*
[c]*Physics Department, Federal University of São Carlos (UFSCar), P.O. Box 676, São Carlos, SP, 13565-905, Brazil*
†Electronic supplementary information (ESI) available. See DOI: 10.1039/c8dt00560e

nanoparticles of around 15 nm and incorporated them into borate and germanate glasses. Both studies did not report the size and shape of the nanoparticles after the melting process.

Although some studies have obtained glasses containing magnetic nanoparticles, the preparation of magnetic glasses with controlled doping and parameters suitable for their functionality in devices, such as good homogeneity and size control for example, has been a major challenge.[18] In particular, because the melt-quenching process occurs at high temperatures, part of the nanoparticles can dissolve during the process. In this way, it highlights the relevance of studying the structural and optical aspects of these materials.

The synthesis of nanoparticles using techniques such as co-precipitation and thermal decomposition, among others, is convenient to synthesize particles of controlled size and morphology. It also allows one to obtain a narrow distribution of nanoparticle sizes, which can be further functionalized by the addition of layers of silica or metallic layers, for example, according to the desired application.[21–23]

Magnetic metal oxide nanoparticles such as cadmium ferrite ($CdFe_2O_4$), which belong to a cubic space group with a normal spinel structure, have been researched due to their excellent chemical stability and applicability in magneto-optical devices, semiconductor sensors, micro-wave absorbers and catalysts.[24–27]

In this context, the aim of this paper is to show the synthesis of cadmium ferrite nanoparticles by co-precipitation and to coat them with silica ($CdFe_2O_4$-SiO_2), which will act as a layer to protect the nanoparticles during the melting process. Later, the particles disperse into the coacervate gel, and finally prepare and characterize a polyphosphate glass containing nanoparticles of cadmium ferrite.

2 Experimental procedures

2.1 Synthesis of $CdFe_2O_4$-SiO_2-600 °C nanoparticles (CdFNPs)

The nanoparticles were synthesized by the coprecipitation method from the aqueous solution of the precursor salts. Initially, 62.5 mL of a 0.005 mol L^{-1} solution of cadmium nitrate tetrahydrate (Sigma-Aldrich, 99%) and 62.5 mL of a 0.01 mol L^{-1} solution of iron nitrate nonahydrate (Sigma-Aldrich, 99%) were mixed. Under stirring, 125 mL of a 1 mol L^{-1} solution of sodium hydroxide (P.A. Synth) was added slowly. The system was kept under a nitrogen atmosphere at a controlled heating rate of 10 °C min^{-1} up to 100 °C.

The total solution was maintained at this temperature for 2 h to complete the formation of $CdFe_2O_4$ nanoparticles. The nanoparticles were washed and then dispersed using ultrasound in ethanol (99%). Subsequently, 3.6 mL of tetraethylorthosilicate (Sigma-Aldrich) and 1.3 mL of 25% ammonium hydroxide solution (P.A. Synth) were added to the dispersion of the nanoparticles. The system remained under mechanical stirring for 24 h under an inert atmosphere. Then, a heat treatment at 600 °C, at room atmosphere, for 5 h was performed to eliminate any organic residue.

2.2 Coacervate preparation

The coacervate was prepared by slowly mixing 4.0 mol L^{-1} of $Na(PO_3)_n$ solutions (Sigma-Aldrich, 99%) with an equal volume of 2.0 mol L^{-1} of $CaCl_2{\cdot}2H_2O$ (2.0 M) (P.A. Synth) solutions under constant stirring. During the addition of calcium chloride to the sodium polyphosphate solution, the formation of a colloidal solution and a liquid–liquid phase separation was observed, evidencing the formation of the coacervate.

2.3 Polyphosphate glasses (PGs)

Four glass samples were prepared, using 12 g of coacervate for each one and by adding the respective quantities of CdFNPs (% in mass) as shown in Table 1.

After homogenization of the sample, which had the consistency of a gel, the mixture was transferred to an alumina crucible. The coacervate and CdFNP mixture was melted at 1000 °C at a heating rate of 10 °C min^{-1}, with a first plateau appearing at 600 °C for 15 min to remove residual water from the coacervate, and a second plateau appearing at 1000 °C for 15 min to homogenization. After that, the samples were cast into a preheated stainless-steel mold at 340 °C. The glasses were maintained at 340 °C for 2 h for annealing. The completion of the samples was achieved by polishing the glasses with SiC sandpaper.

2.4 $CdFe_2O_4$, CdFNP and PG characterization

X-ray powder diffraction analyses for the "as prepared" $CdFe_2O_4$ nanoparticles, CdFNPs and PGs were carried out with a Bruker D8 Advance diffractometer operating with a Ni filtered CuKα radiation source at 2θ angle ranging from 10 to 80° with a step pass of 0.02° and a step time of 2 s. Transmission electron microscopy (TEM) and scanning transmission electron microscopy (STEM) imaging using an annular dark field (ADF) detector followed by elemental mapping through EDS (energy dispersive spectroscopy) were carried out using a Tecnai FEI G^2 TEM/STEM 200 kV equipped with an energy dispersive X-ray detector. Samples were prepared using 0.1 mg of CdFNPs or PG samples containing nanoparticles. After grinding, the powder was dispersed in 1 mL of isopropyl alcohol using ultrasound. Some drops of this suspension were applied on a copper grid coated with a carbon film. The spectra in the infrared region (4000–500 cm^{-1}) were obtained using a PerkinElmer 2000 equipment, in transmission mode, with 2 cm^{-1} resolution and 32 reading scans. Magnetization measurements were performed using a VSM-SQUID (vibration sample magnetometer with a superconducting quantum inter-

Table 1 Phosphate glass samples obtained with different concentrations of the CdFNPs and the label given for samples

Sample label	% in mass of CdFNPs
PG	0
PG-1% CdFNPs	1
PG-4% CdFNPs	4
PG-8% CdFNPs	8

ference device) MPMS 3 by Quantum Design to CdFNPs and PG-8% CdFNPs up to 400 K, with application of a magnetic field of 100 Oe. Differential scanning calorimetry (DSC) measurements were carried out using a DSC404 F3 Pegasus equipment from NETZSCH to study the PG samples. Small pieces of glasses, of typically 15 mg, were heated in a platinum crucible from 25 to 750 °C at a heating rate of 10 °C min^{-1} under a N_2 atmosphere (70 mL min^{-1}) and the estimate error is ±2 °C for T_g and T_x. Raman scattering spectra were recorded at room temperature in a frequency range from 200 to 1500 cm^{-1} using a HORIBA Jobin Yvon model LabRAM HR micro Raman apparatus equipped with a 632.8 nm laser, delivering 17 mW. High resolution solid state NMR experiments were carried out at room temperature on a Bruker Avance III 400WB HD spectrometer, using a 4 mm triple MAS-NMR probe at a spinning speed of 14 kHz. ^{31}P NMR measurements were carried out at 162.0 MHz using 90° pulses of 3.2 ms length and a recycle delay of 300 s. Chemical shifts are reported relative to 85% H_3PO_4. Signal deconvolutions into the Gaussian components were performed using the DMFIT software package.[28] The refractive indices of the samples were measured on a MATRICON model 2010 equipment, and the length of the incident radiation was 632.8 nm (red) and the estimate error is ±0.001. UV-Vis absorption and transmission spectra (in the spectral range from 200 to 1300 nm) were recorded using a Varian Cary 5000 UV-Vis-Near infrared (NIR) spectrophotometer, on the polished samples of 2 mm in thickness.

3 Results and discussion

3.1 $CdFe_2O_4$ nanoparticles and CdFNPs characterization

The XRD patterns of the as-synthesized $CdFe_2O_4$ nanoparticles and CdFNPs are shown in Fig. 1(a). The presence of the 222, 311, 422, 511, 440 and 620 reflection planes in the diffraction pattern matches well with the standard (JCPDS 22-1063), confirming that the obtained nanoparticles have an *Fd3m* (227) cubic spinel structure. The reflection plane 311 of cadmium ferrite (34.4°) is shifted to a smaller 2θ value in comparison with the same plane of Fe_3O_4 (35.4°), due to the incorporation of the Cd atoms in the structure. The low intensity diffraction peak at 42.5° is assigned to the 400 plane of Fe_3O_4 according to the standard (JCPDS 19-0629).

Nanoparticles were coated with a silica layer to protect them during the glass preparation, that is, the glass melting. After silica layer coating, a heat treatment was performed at 600 °C to eliminate the organic compounds that could remain after several washes.

The TEM image (Fig. 1(b)) shows small spherical particles of CdFNPs with a size distribution ranging between 2.5 and 5.0 nm and with an average diameter of 3.9 nm. It is possible to observe that the nanoparticles are not surrounded by the silica layer in a monodisperse manner, but into the silica agglomerates, where the thickness of the silica layer is different at each point.

This behavior is due to the magnetic interactions that entail a tendency for attraction between the nanoparticles,[29] as

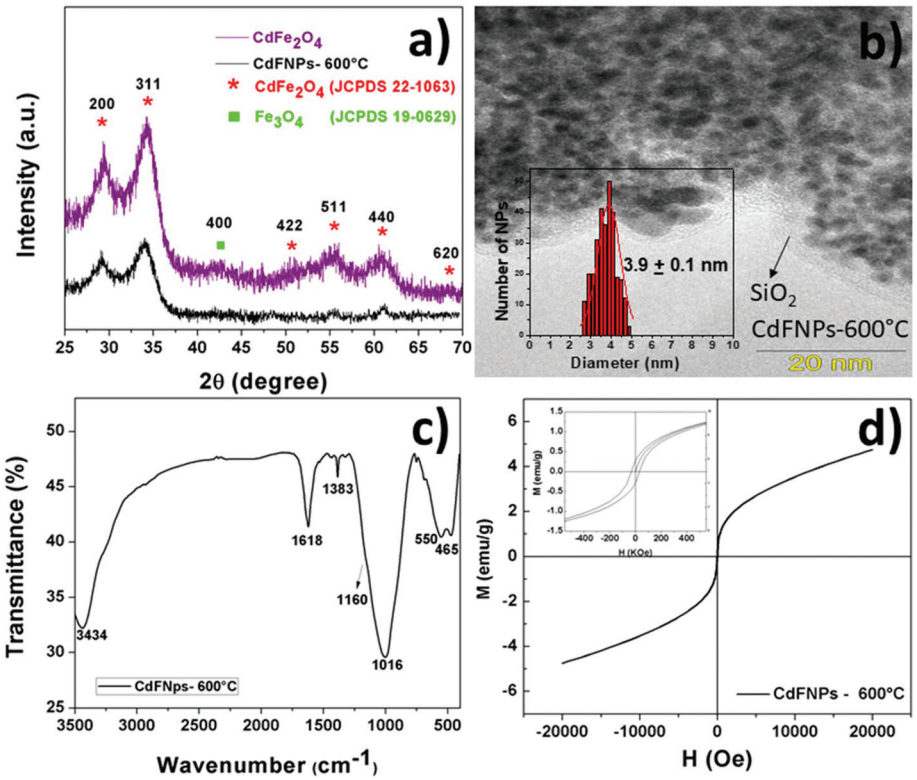

Fig. 1 Characterization of cadmium ferrite nanoparticles: (a) XRD patterns of $CdFe_2O_4$ nanoparticles and CdFNPs; (b) TEM image of CdFNPs; (c) infrared spectrum of CdFNPs; and (d) the *M*–*H* curve of CdFNPs.

well as the surfactant-free synthesis, chosen in order to avoid the remaining organic compounds between the nanoparticle and silica layer which can cause bubbles during the synthesis of the glass.

Fig. 1(c) shows the infrared spectrum of CdFNPs. Spinel crystalline phases, especially ferrites, have characteristic bands attributed to the stretching of the metal–oxide vibrations in the octahedral (400–450 cm^{-1}) and tetrahedral (540–600 cm^{-1}) positions.[30] In the spectrum, the band observed at 550 cm^{-1} is assigned to the $M^{2+}_{(tetrahedral)}$–O stretch, but the band referring to the $M^{2+}_{(octahedral)}$–O is enveloped by the band at 465 cm^{-1} associated with Si–O–Si and O–Si–O torsional motions.

The characteristic bands of the silica network usually appear at 1086 cm^{-1} with high intensity and one shoulder at 1160 cm^{-1}, assigned to the asymmetric stretching of the Si–O–Si bonds of the SiO_4 tetrahedron and at 810 cm^{-1} associated with the symmetric stretching of the Si–O–Si bonds.[31] In the spectrum, these bands composed of a broadband from 770 to 1250 cm^{-1}. The band at 1383 cm^{-1} is associated with the nitrate species remaining on the surface of the particle.[32] The bands at 1618 and 3434 cm^{-1} are assigned to the H–O–H torsion and the stretching modes of the free or absorbed water, respectively.[30]

The nanoparticles were characterized magnetically by the SQUID technique, which measures the magnetization variation of the sample as a function of the applied magnetic field. From Fig. 1(d), it can be observed that the CdFNPs showed no hysteresis and no saturation in the range investigated (−20 kOe up to 20 kOe), indicating that the nanoparticles are superparamagnetic.[26] Kaur *et al.* performed magnetic measurements in the same range of the magnetic field for $CdFe_2O_4$ nanoparticles of 12–27 nm and obtained similar results.[26] This behavior is attributed to the redistribution of the Fe^{3+} ions between the octahedral and tetrahedral sites, which occurs for cadmium ferrite nanoparticles differently from bulk, where the Cd^{2+} atoms, preferentially, occupy tetrahedral sites.

The low magnetization values up to the investigated field (4.78 emu g^{-1}) may be influenced by the diamagnetic inorganic coating through the magnetic dilution phenomenon. This lower value could also be attributed to the surface contribution of spin canting and surface disorder, and moreover nanoparticles synthesized by the coprecipitation method may have crystal defects.[33–35] The small hysteresis is due to the spin coupling phenomena and is not sufficient to characterize it as a hard magnetic material.[33]

3.2 Characterization of PGs containing CdFNPs

The coacervate gel makes it easy to incorporate and homogenize nanoparticles into the material. The phosphate glasses are usually very hygroscopic, but it is interesting to emphasize that the samples obtained do not show any sign of hygroscopicity, even if they are not stored in a desiccator.

Fig. 2 illustrates the coacervation process and subsequent obtainment of glasses containing CdFNPs, and an image of

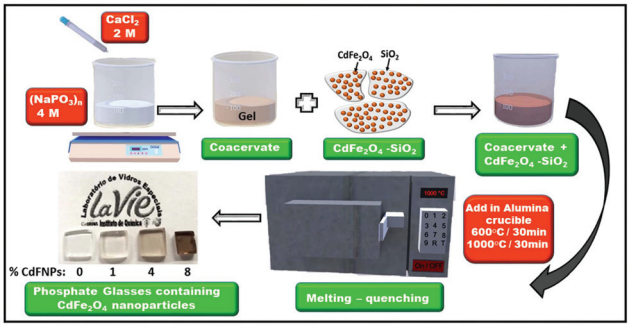

Fig. 2 Illustration of the coacervation process, subsequent incorporation of the nanoparticles and the obtained glasses containing CdFNPs.

the vitreous samples containing 0, 1, 4 and 8% CdFNPs obtained. All glass samples are fully transparent.

The PG glass sample is colorless and the addition of the nanoparticles turns it amber, which is characteristic of the presence of iron ions.[36] The color is more intense from the sample containing 4% nanoparticles. This suggests that some of the nanoparticles added dissolve in the matrix.

From the TEM images, it is possible to observe that the nanoparticles were successfully incorporated into the matrix. Fig. 3(a) shows the PG-4% CdFNPs sample, with part of the nanoparticles more clustered and others more dispersed in the vitreous matrix.

A histogram was obtained from the TEM image of Fig. 3(a), with a count of 42 nanoparticles (since the amount of nanoparticles present in the glass sample is much lower than that presented in the TEM images of nanoparticles (Fig. 1b)). The calculated size distribution has diameters between 2.1 and 4.2 nm and a mean diameter of 2.8 nm ± 0.1. Compared with the CdFNPs prior to incorporation, the mean diameter undergoes a 29% reduction (from 3.9 to 2.8 nm), indicating that the size of the nanoparticles reduces during the melting of the material.

In the PG-8% CdFNPs sample (Fig. 3b), some agglomerates of silica containing the nanoparticles can be noted.

The polyphosphate matrix has proven to be a good host for the nanoparticles. A large amount of nanoparticles is observed in the whole piece of glass analyzed as shown in Fig. 3(b) and (c) without inducing further crystallization of the sample.

The X-ray diffractograms of the PG and PGs containing CdFNPs (see S1†) presented only the diffraction halo characteristic of amorphous materials. It was expected that after the incorporation of the nanoparticles into the glass matrix it was not possible to identify the cadmium ferrite peaks, since the amount of $CdFe_2O_4$ is very small, compared to the amount of silica and phosphate, and is dispersed in the matrix making it difficult for diffraction.

This is very interesting since a large amount of nanocrystals was introduced into the sample, which could induce crystallization, because being very light, the volume of the nanoparticles added is very large. The elemental mapping through EDS (see S2†) shows the distribution of the Fe, Cd, Si and O elements for the PG-4% CdFNPs and PG-8% CdFNPs samples.

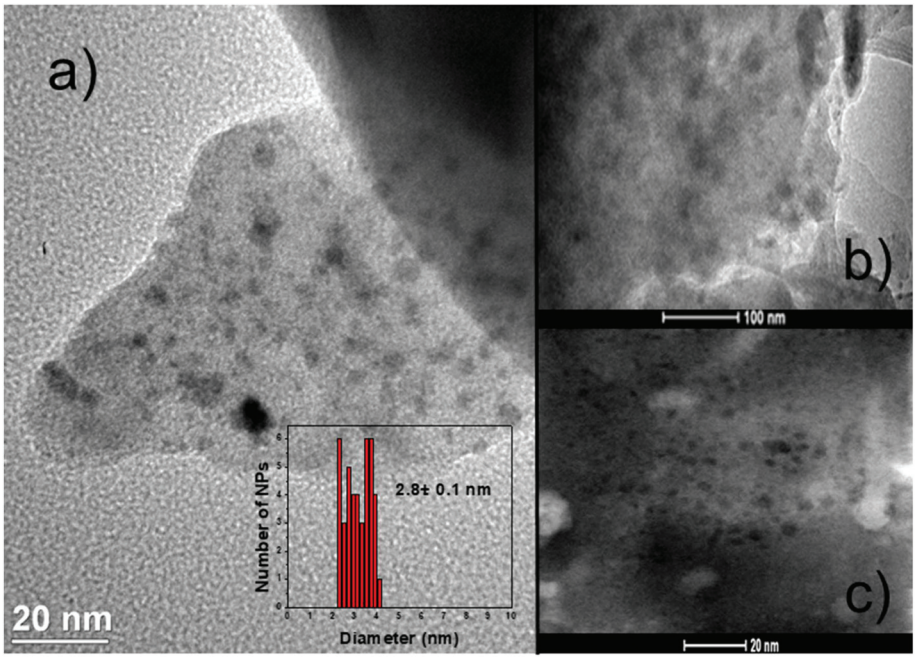

Fig. 3 TEM images of (a) PG-4% CdFNPs; (b) and (c) PG-8% CdFNPs.

3.3 Structural characterization

The ^{31}P MAS NMR technique can be used to study the phosphate species present in the material. The complication (and challenge) of NMR studies in materials containing paramagnetic compounds consists of the fact that the NMR signals may not be observed due to the dipolar and lifetime broadening phenomena. The structures of the phosphate glasses are generally classified using the terminology Q^n,[37] where the number of oxygens linked to the phosphorus atoms per tetrahedron is represented by n, and can assume values of 0, 1, 2 and 3 (this terminology also applies to silicate tetrahedra). The ^{31}P MAS NMR spectra of the analyzed glasses are presented in Fig. 4(a) and Table 2 shows the parameters obtained from the deconvolution model.

It is possible to observe that the phosphate glasses prepared from the coacervate present two resonance lines at −23.8 and −7.6 ppm, attributed to Q^2 and Q^1 species, respectively. The spectra of the glasses containing CdFNPs show a loss of resolution, suggesting that both the Q^2 and Q^1 signals are significantly broadened by paramagnetic interactions of the ^{31}P nuclei with the Fe^{3+} ion electron spins. The addition of CdFNPs results in a decrease of the Q^2 species, while the percentage of the Q^1 species increases with increasing CdFNPs, which means that the incorporation of the nanoparticles causes the breakage of the P–O–P bridges. A new resonance line was observed at −39.6 ppm and it can be attributed to a phosphate tetrahedral linkage to the silicate species, P–O–Si.[38] These new species increase with increasing the concentration of CdFNPs. The ^{31}P MAS NMR results suggest that the silicate layer of the CdFNPs is partially dissolved in the phosphate network of the glasses and are in agreement with the previous TEM results, where a decrease in the nanoparticle size was observed after incorporation into the glasses.

Fig. 4(b) shows the Raman spectra of the PG which present two main vibrational modes at 691 and 1174 cm^{-1}, assigned to the symmetrical stretches ν_s(P–$O_{bridged}$) and ν_s(P–$O_{terminal}$), respectively, and the O–P–O bending motions in the range of 400–300 cm^{-1}.[39] The increase in the concentration of CdFNPs in the phosphate matrix results in a slight shift of the ν_s(P–O_b) band to higher frequencies and the shift of the ν_s(P–O_t) band to lower frequencies.

The bands in the range between 1100 and 860 cm^{-1} are assigned to the asymmetric vibration of the SiO_4 tetrahedral units according to the literature.[40] The Raman bands at about 1085 cm^{-1} and 1025 cm^{-1} have been assigned to the stretching vibrations of a single non-bridging oxygen atom (NBO) in a silicate tetrahedron and to antisymmetric stretching vibrations of the Si–O and P–O bonds in the Si–O–Si and P–O–Si linkages, respectively.[40,41] The band at about 965 cm^{-1} is assigned to the Si–O stretching mode in the Q^2 silicate units while the band at 480 cm^{-1} is assigned to the bending vibrations of the oxygen bridges such as O–Si–O.[41,42]

The NMR and Raman results are in agreement, showing that the polyphosphate chains are being broken while some of the silicon atoms have been incorporated into the phosphate glass network.

3.4 Thermal analysis of glasses

The vitreous samples were studied by thermal analysis (DSC), which allows the determination of the characteristic temperatures of the glasses: the glass transition temperature (T_g),

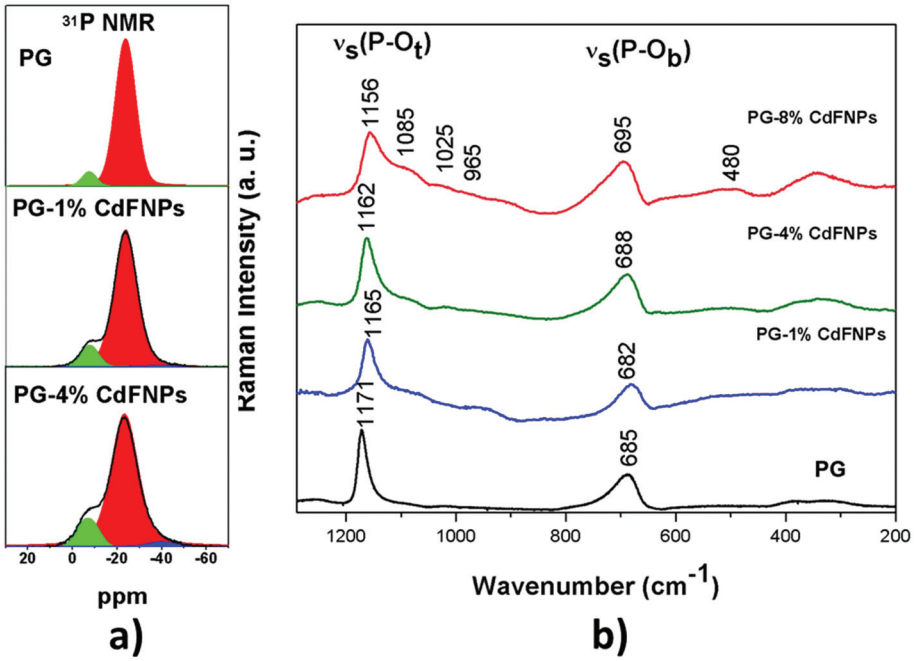

Fig. 4 (a) ^{31}P NMR spectra obtained for PG and samples containing 1 and 4% CdFNPs (experimental curves and fitted curves) and (b) Raman spectra obtained for the vitreous samples.

Table 2 Deconvolution results (chemical shifts, δ_{iso} ±0.5 ppm, fractional areas, ±2%, and width) of the ^{31}P MAS-NMR spectra obtained on PG glasses

Samples	Chemical shift (ppm)	Species	Fractional areas (%)	FWHM[a] (ppm)
PG	−23.8	Q^2	95.4	10.5
	−7.5	Q^1	4.6	7.4
PG-1% CdFNPs	−23.8	Q^2	92.8	14.7
	−7.6	Q^1	6.8	10.7
	−39.6	P–O–Si	0.4	
PG-4% CdFNPs	−23.3	Q^2	90.0	14.5
	−6.9	Q^1	8.6	10.4
	−39.6	P–O–Si	1.4	

[a] Full width at half maximum.

onset of crystallization temperature (T_x) and maximum crystallization temperature (T_p).

The DSC curves for the matrix and for the glasses containing CdFNPs are shown in Fig. 5(a), from which one can observe that the T_g increases with the increasing nanoparticle content. Such behavior is related to an increase in the degree of structural rigidity, assigned to the formation of the Si–O–P bonds and confirmed by NMR and Raman data.

While the addition of nanoparticles breaks the polyphosphate chains, leading to a decrease in the T_g, new P–O–Si bonds are being formed promoting the linkage between the polyphosphate chains resulting in an increase of the vitreous network connectivity.

The $T_x - T_g$, which is the thermal stability against the crystallization parameter, increases with the increasing concentration of CdFNPs (Fig. 5(b)). No evidence of crystallization was found for the samples containing 1, 4 and 8% nanoparticles, showing that the glasses acquired enormous stability against crystallization. This fact is important for technological applications, especially for the production of optical devices, since large values of $T_x - T_g$ allow the preparation of large samples. The values of T_g, T_x, and T_p and the thermal stability parameter ($T_x - T_g$) are shown in Table 1 in S3.†

3.5 Optical measurements

The value of the refractive index is important in the study of optical properties. The characterization of the glasses was performed using the prism coupling technique, M-lines spectroscopy, at a wavelength of 632.8 nm. The refractive index values of the vitreous samples are listed in Table 3.

The increase in the nanoparticle concentration increases linearly with the refractive index. Such behavior can be attributed to the presence of Fe^{3+} ions, which due to their atomic radius of 64.5 pm, have the ability to polarize neighboring atoms.[43]

Spectroscopy in the UV-Vis region was used to obtain absorption and transmittance spectra. From Fig. 6(a), it can be observed that samples with 1, 4 and 8% nanoparticles have bands at 415 nm (for the samples containing 1 and 4% nanoparticles) and 520 nm, which can be assigned to the Fe^{3+} ions, while the broadband at 1025 nm is characteristic of the Fe^{2+} ions in the matrix.[36]

The iron ions can coexist in the Fe^{2+} and Fe^{3+} forms in the vitreous matrix; the balance between the two species depends on the glass composition, iron concentration and sample

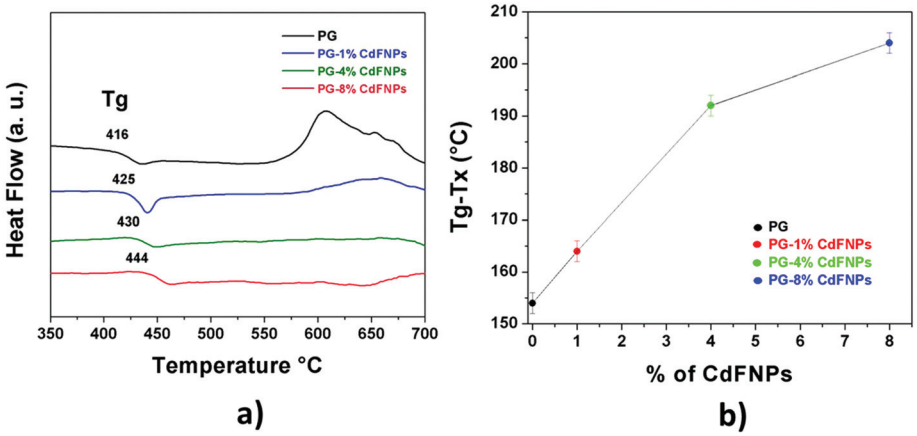

Fig. 5 (a) DSC curves of glasses and (b) thermal stability parameters ($T_x - T_g$) values for the glasses (the line is just a guide to the eye).

Table 3 Refractive index and optical band gap energy values

Sample	Refractive index	E_{opt} (eV)
PG	1.527	3.42
PG-1% CdFNPs	1.540	3.01
PG-4% CdFNPs	1.548	2.98
PG-8% CdFNPs	1.557	2.81

preparation conditions.[44] The presence of the Fe^{2+} and Fe^{3+} bands confirms that part of the incorporated nanoparticles dissolves during the melting process and is a consequence of the high melting temperature used to obtain the glasses.

Fig. 6(b) shows the transmission spectra of the glasses which show a red shift of the absorption edge as a function of the content of CdFNPs. The decrease in transmittance is due to the scattering caused by the silica agglomerates which remain inside the glass after melting.

The absorption coefficients of the glasses are determined in the region of strong absorption, which involves optical transitions between the valence and conduction bands. The absorption limit in the visible region is usually called band gap energy, and its value can be obtained from the transmission spectra using the PARAV software. In this software the transmission spectrum of the glasses is inserted and, knowing the values of the refractive indices and thicknesses of the glasses, we can obtain the values of the parameters necessary to plot a graph of $(ahv)^{1/2}$ as a function of the energy of the photon (E).[45]

Table 3 shows the values of the optical band gap (E_{opt}) of the glasses determined from a tangent drawn at the intersection of the curve $(ahv)^{1/2} \times E$.

E_{opt} is strongly dependent on the electronic structure and decreases with the increasing nanoparticle concentration, which can be attributed to the fact that the nanoparticles introduce new energy levels between the valence band and matrix conduction band, showing that the band gap of the polyphosphate matrix is sensitive to the incorporation of CdFNPs.

The same behavior was observed by Winadarto *et al.* in their work in which they added natural Fe_3O_4 nanoparticles into a glassy matrix $(80 - x)TeO_2 - xFe_3O_4 - 20ZnO$ $(0 \leq x \leq 2)$.

3.6 Magnetic measurements

The PG and PG-8% CdFNP samples were also characterized by the VSM-SQUID technique. The PG presents a diamagnetic behavior in all ranges of temperature as shown in Fig. 7(a) and (b). For the PG-8% CdFNPs sample, a clear paramagnetic behavior was observed.

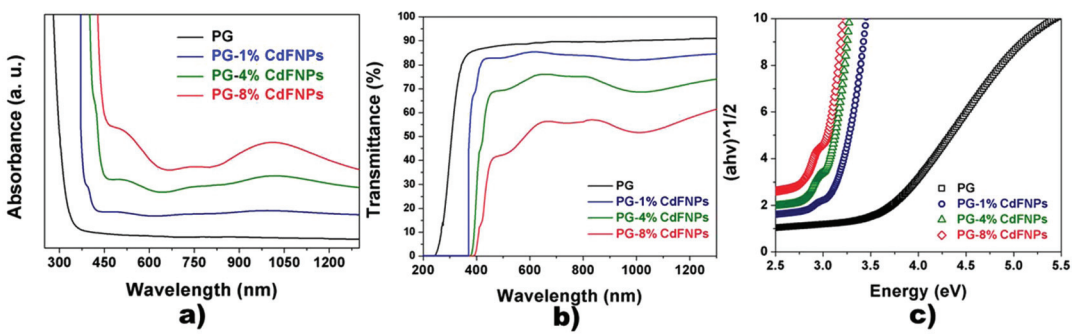

Fig. 6 (a) Absorbance spectra; (b) transmittance spectra; and (c) graph of $(ahv)^{1/2}$ as a function of the photon energy obtained for the glasses.

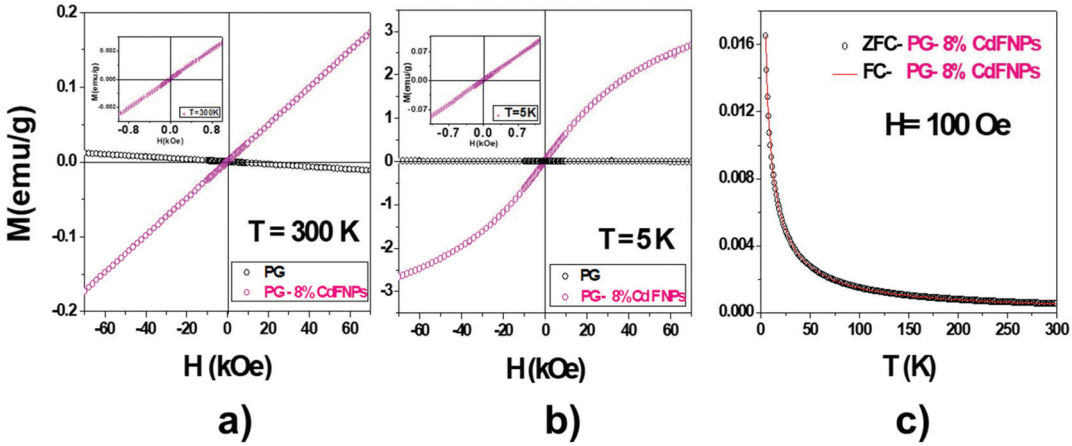

Fig. 7 Magnetization as a function of applied magnetic field for PG and the PG-8% CdFNP sample in (a) T = 300 K; (b) T = 5 K; and (c) FC–ZFC magnetization curves measured at H = 100 Oe.

The experiment of dependence of magnetization as a function of temperature under a magnetic field of 100 Oe was performed to verify if there is any possible interaction between the magnetic moments, which would be characterized by a difference between the two curves (Fig. 7(c)). As the data indicate, there was no irreversibility for any of the fields applied, reinforcing the conclusion that the sample has a paramagnetic behavior, although the previously prepared cadmium ferrite nanoparticles show a superparamagnetic behavior.

Anigrahawati and Ghoshal[16] reported in their work the preparation of vitreous samples composed of $(69 - x)P_2O_5 - 30ZnO - 1Er_2O_3 - (x)Fe_3O_4$ where x is the percentage in mole (0.5, 1.0, 1.5 and 2.0%) of natural Fe_3O_4 nanoparticles. The nanoparticle sizes determined in the glass were between 26 and 31 nm. The magnetic measurements of the nanoparticles prior to incorporation into the glass indicated a ferrimagnetic behavior. For the vitreous samples containing 0.5 and 1.0 mol%, the samples presented a linear paramagnetic behavior with the applied field, but for the samples containing 1.0, 1.5 and 2.0 mol%, a narrow hysteresis was observed due to the presence of clusters of Fe_3O_4.[16]

In this way, the paramagnetic behavior obtained in our sample is attributed to the fact that the nanoparticles are extremely small (less than 5 nm) and are dispersed in a diamagnetic matrix causing a magnetic dilution effect, which leads to no interaction between the particles. In addition, the dissolution of part of the nanoparticles in the matrix contributes to this behavior since the Fe^{3+} ions are paramagnetic.

However, this paramagnetic behavior may influence the other properties of the material, for example, in magneto-optical measurements it may show interesting effects. From these results, we can adjust the nanoparticle synthesis parameters to obtain larger nanoparticles and to improve the nanoparticle coating, to avoid their dissolution, in order to achieve satisfactory magnetic results since the incorporation method of the nanoparticles was satisfactory.

4. Conclusion

In this work, the gel coacervate was used as a precursor for homogeneous mixing of the CdFNPs, and then this material was melted and phosphate glasses were obtained. We have shown that the method of protection of the nanoparticles with a silica layer is efficient and the incorporation into the vitreous matrix was satisfactory, as shown in the TEM images. The thermal and structural investigations are in agreement and show that the incorporation of CdFNPs promotes the breaking of the phosphate chains and the formation of new P–O–Si bonds that confer greater thermal stability to the matrix, this fact is very important in the fabrication of optical fibers. The optical measurements indicate that part of CdFNPs dissolves during the melting process, showing that it is necessary to improve the quality of the silica coating in order to avoid that. Our results of the incorporation methodology may contribute towards the development of glasses containing nanoparticles useful for magneto-optical devices.

Conflicts of interest

There are no conflicts to declare.

Acknowledgements

The authors are grateful to the Brazilian funding agencies, CNPq (141258/2014-4) and São Paulo Research Foundation FAPESP (grant numbers #2013/07793-6 and 09/54082-2).

References

1 R. K. Bron, *Non-Cryst. Solids*, 2000, **263 & 264**, 1–28.

2 M. Karabulut, E. Melnik, R. Stefan, G. K. Marasinghe, C. S. Ray, C. R. Kurkjian and D. E. Day, *J. Non-Cryst. Solids*, 2001, **288**, 8–17.
3 G. Willot, F. Gomez, P. Vast, V. Andries, M. Martinez, Y. Messaddeq and M. Poulan, *C. R. Chim.*, 2002, **5**, 899–906.
4 F. Gomez and P. Vast, *Phosphorus Res. Bull.*, 2000, **11**, 61–68.
5 T. Umegaki and T. Kanazawa, *Bull. Chem. Soc. Jpn.*, 1973, **46**, 3587–3588.
6 T. Umegaki, Y. Nakayama and T. Kanazawa, *Bull. Chem. Soc. Jpn.*, 1976, **49**, 2105–2107.
7 M. A. P. Silva, D. F. Franco and L. F. C. De Oliveira, *J. Phys. Chem. A*, 2008, **112**, 5385–5389.
8 D. F. Franco, D. Manzani, H. S. Barud, S. G. Antonio, L. F. C. de Oliveira, M. A. P. Silva, S. J. L. Ribeiro and M. Nalin, *RSC Adv.*, 2016, **6**, 91150–91156.
9 G. Palavit, L. Montagne and R. Delaval, *J. Non-Cryst. Solids*, 1995, **189**, 277–282.
10 R. Berger, J. Kliava and J. C. Bissey, *J. Appl. Phys.*, 2000, **87**, 7389.
11 I. Edelman and J. Kliava, *Phys. Status Solidi*, 2009, **246**, 2216.
12 C. Worsch, M. Buttner, P. Schaaf, R. Harizanova, C. Russel, F. Schmidl and P. Seidel, *J. Mater. Sci.*, 2013, **48**, 2299.
13 J. Shenga, K. Kadonoa, Y. Utagawab and T. Yazawaa, *Appl. Radiat. Isot.*, 2002, **56**, 621.
14 J. Sheng, J. Zhang and L. Qiao, *J. Non-Cryst. Solids*, 2006, **352**, 2914.
15 J. Zhanga, W. Dongb, J. Shenga, J. Zhenga, J. Lia, L. Qiaoa and L. Jianga, *J. Cryst. Growth*, 2008, **310**, 234.
16 P. Anigrahawati, M. R. Sahar and S. K. Ghoshal, *Mater. Chem. Phys.*, 2015, **155**, 155–161.
17 W. Widanarto, M. R. Sahar, S. K. Ghoshal, R. Arifin, M. S. Rohani and K. Hamzah, *J. Magn. Magn. Mater.*, 2013, **326**, 123–128.
18 W. Widanarto, M. R. Sahar, S. K. Ghoshal, R. Arifin, M. S. Rohani and M. Effendi, *Mater. Lett.*, 2013, **108**, 289–292.
19 H. K. Farag and M. A. Marzouk, *J. Mater. Sci.: Mater. Electron.*, 2017, **28**, 15480–15487.
20 Q. Chen, L. Wan, Q. Chen and M. Zhang, *Adv. Mater. Res.*, 2011, **271**, 13–18.
21 S. Laurent, D. Forge, M. Port, A. Roch, C. Robic, L. V. Elst and R. N. Muller, *Chem. Rev.*, 2008, **108**, 2064–2110.
22 W. Oh and J. P. Liu, *J. Magn.*, 2006, **11**, 123–125.
23 L. Xiong, X. Du, B. Shi, J. Bi, F. Kleitz and S. Z. Qiao, *J. Mater. Chem. B*, 2015, **3**, 1712–1721.
24 X. Lou, S. Liu, D. Shi and M. Chu, *Mater. Chem. Phys.*, 2007, **105**, 67–70.
25 A. F. Bakuzis, K. Skeff Neto, P. P. Gravina, L. C. Figueiredo and P. C. Morais, *Appl. Phys. Lett.*, 2004, **84**, 2355–2357.
26 H. Kaur, J. Singh and B. S. Randhawa, *Ceram. Int.*, 2014, **40**, 12235–12243.
27 M. Naseri, *J. Magn. Magn. Mater.*, 2015, **392**, 107–113.
28 D. Massiot, F. Fayon, M. Capron, I. King, S. Le Calve, B. Alonso, B. B. Durand, Z. Gan and G. Hoatson, *Magn. Reson. Chem.*, 2002, **40**, 70–76.
29 M. H. Carvalho, R. J. S. Lima, C. T. Meneses, W. S. D. Folly, V. H. V. Sarmento, A. A. Coelho and J. G. S. Duque, *J. Appl. Phys.*, 2016, **119**, 93909.
30 K. N. Harish, H. S. Bhojya Naik, P. N. Prashanth kumar and R. Viswanath, *Catal. Sci. Technol.*, 2012, **2**, 1033–1039.
31 J. B. Silva, *J. Sol-Gel Sci. Technol.*, 2005, **35**, 115–122.
32 M. Saravanan and T. C. S. Girisun, *Mater. Chem. Phys.*, 2015, **160**, 413–419.
33 B. D. Cullity and C. D. Graham, *Introduction to magnetic materials*, Wiley-IEEE Press, 2nd edn, 2008.
34 R. H. Kodama, *J. Magn. Magn. Mater.*, 1999, **200**, 359–372.
35 P. K. Nayak, *Mater. Chem. Phys.*, 2008, **112**, 24–26.
36 J. M. F. Navarro, *El Vidrio*, CSIC Press, Madrid, Spain, 3rd edn, 2003.
37 M. O'Keeffe and A. Navrotsky, *Structure and Bonding in Crystals*, Academic Press, New York, 1981.
38 N. J. Clayden, S. Esposito, P. Pernice and A. Aronne, *J. Mater. Chem.*, 2001, **11**, 936–943.
39 M. A. P. Silva, D. F. Franco, A. R. Brandão, H. S. Barud, F. A. Dias Filho, S. J. L. Ribeiro, Y. Messaddeq and L. F. C. De Oliveira, *Mater. Chem. Phys.*, 2010, **124**, 547–551.
40 S. Agathopoulos, D. U. Tulyaganov, J. M. G. Ventura, S. Kannan, A. Saranti, M. A. Karakassides and J. M. F. Ferreira, *J. Non-Cryst. Solids*, 2006, **352**, 322.
41 V. G. Plotnichenko, V. O. Sokolov, V. V. Koltashev and E. M. Dianov, *J. Non-Cryst. Solids*, 2002, **306**, 209–226.
42 M. Szumera, *Spectrochim. Acta, Part A*, 2014, **130**, 1–6.
43 D. R. Shannon, *Acta Crystallogr., Sect. A: Cryst. Phys., Diffr., Theor. Gen. Crystallogr.*, 1976, **32**, 751.
44 I. Ardelean, M. Toderas and S. Filip, *J. Magn. Magn. Mater.*, 2004, **272**, 339–341.
45 A. Ganjoo and R. Gollovchak, *J. Optoelectron. Adv. Mater.*, 2008, **10**, 1328–1332.